Magnetic Field Perturbation and Magnetic Stress Analysis Due to a Ferromagnetic First Wall

doi: 10.1109/20.106333

Magnetic Field Perturbation and Magnetic Stress Analysis due to a Ferromagnetic First Wall

T.Ohira, T.Takagi*, K.Miya**
*T.Horie** and Y.Seki***

*Nuclear Engineering Research Laboratory
The Faculty of Engineering
The University of Tokyo
Tokai, Ibaraki, 319-11, Japan
**Japan Atomic Energy Research Institute
Naka-machi, Ibaraki, 311-02, Japan

ABSTRACT

Based on a magnetization integral equation we developed a magnetic field analysis method for three dimensional complicated components formed by thin shells. It was applied to the analysis of magnetic induction and stress in a ferromagnetic first wall. As a result we found the wall could be used in a fusion reactor without much problem.

1. Introduction

A ferromagnetic material(9Cr-1Mo,HT-9) is likely to prove extremely useful for a first wall of a fusion power reactor because of low rate of irradiation swelling. But the problem of how much magnetic induction and stress is induced in the material in high field beyond the saturation has not been studied to any extent [1-3] . In view of the design of the first wall we are extremely concerned about it. Then, in this study we developed a thin-plate approximation analysis method to evaluate magnetic field in three dimensional complicated components formed by thin shells and analyzed magnetic induction and stress in the first wall.

2. Basic Theory

2.1. Magnetization Integral Equation

The magnetic field intensity can be separated into two parts

$$\boldsymbol{H} = \boldsymbol{H}_S + \boldsymbol{H}_M, \tag{1}$$

the part, $\boldsymbol{H}_S$, being directly the result of the current sources present whereas $\boldsymbol{H}_M$ is regarded as being due to magnetization vector $\boldsymbol{M}$ induced in the material. If it is assumed that $\boldsymbol{H}_S$ is entirely independent of the material properties then this vector must be determined by the relationship applying to distributed currents in free space,

$$\boldsymbol{H}_S(\boldsymbol{r}) = \frac{1}{4\pi}\int_{\Omega_j} \frac{\boldsymbol{J}(\boldsymbol{r}') \times (\boldsymbol{r}-\boldsymbol{r}')}{|\boldsymbol{r}-\boldsymbol{r}'|^3} d\Omega' . \tag{2}$$

The vectors $\boldsymbol{r}$ and $\boldsymbol{r}'$ are, respectively, field and source point vectors referred to a common origin. The integration is over the region of space Ω_j which contains all the current sources and the operation is performed with respect to the variable $\boldsymbol{r}' = (x', y', z')$. On the other hand, $\boldsymbol{H}_M$ can be written as follows, [4-6]

$$\boldsymbol{H}_M(\boldsymbol{r}) = \frac{1}{4\pi}\nabla\int_{\Omega_M} \frac{\boldsymbol{M}(\boldsymbol{r}')\cdot(\boldsymbol{r}-\boldsymbol{r}')}{|\boldsymbol{r}-\boldsymbol{r}'|^3} d\Omega', \tag{3}$$

the gradient operator ∇ here of course being with respect to the unprimed coordinates $\boldsymbol{r} = (x, y, z)$. We can derive the following equation from Eqs.(1)-(3),

$$\boldsymbol{M}(\boldsymbol{r}) = \frac{\chi(\boldsymbol{r})}{4\pi}\left[\int_{\Omega_j} \frac{\boldsymbol{J}(\boldsymbol{r}')\times(\boldsymbol{r}-\boldsymbol{r}')}{|\boldsymbol{r}-\boldsymbol{r}'|^3} d\Omega' - \nabla\int_{\Omega_M} \frac{\boldsymbol{M}(\boldsymbol{r}')\cdot(\boldsymbol{r}-\boldsymbol{r}')}{|\boldsymbol{r}-\boldsymbol{r}'|^3} d\Omega'\right], \tag{4}$$

where χ denotes the susceptibility of the material.

2.2. Discretization

The problem of determining the magnetic field in three dimensional component formed by thin ferromagnetic plates close to current- carrying circular loops is considered. It is shown schematically in Fig.1. If we divide the ferromagnetic plates into N triangular prism elements and treat the magnetization as constant over each , from Eq.(3) we obtain the following equation for the field at the center of element k due to the magnetization of all the elements :

$$\boldsymbol{H}_{Mk} = \sum_{l=1}^{N} \boldsymbol{C}_{kl}\boldsymbol{M}_l, \quad k=1,2,...,N, \tag{5}$$

where $\boldsymbol{H}_{Mk}$ and $\boldsymbol{M}_l$ are three component vectors, and each $\boldsymbol{C}_{kl}$ factor depends only on the geometry of the field point

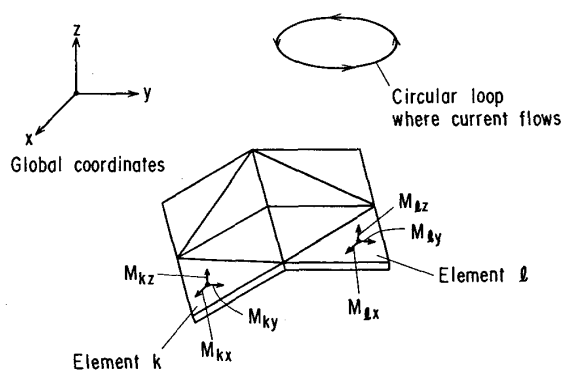

Fig. 1 A schematic view of 3-D components formed by thin ferromagnetic plates close to a current-carrying circular loop

0018-9464/90/0300-0379$01.00 © 1990 IEEE

and source element.

Thus the problem of determining the magnetization has been discretized, for now it may be written, from Eq.(4),

$$\boldsymbol{M}_k = \chi(r_k)\left[\boldsymbol{H}_{Sk} + \sum_{l=1}^{N} C_{kl}\boldsymbol{M}_l\right], \tag{6}$$

or

$$\sum_{l=1}^{N}\left[C_{kl} - \frac{\delta_{kl}}{\chi(r_k)}\right]\boldsymbol{M}_l = -\boldsymbol{H}_{Sk}. \tag{7}$$

$\boldsymbol{H}_{Sk}$ can be calculated from the Biot-Savart law and the *kronecker delta* $\delta_{kl} = 1$, $k=l$ or $\delta_{kl} = 0$, $k \neq l$, is introduced. Equation (7) is of matrix form and can be inverted to yield $\boldsymbol{M}_l$ [7].

If it is wished to take into account nonlinear material properties, Eq.(7) can be solved iteratively starting from a guessed solution which, given B-H curves for the material, enables $\chi(r_k)$ to be estimated initially.

If we let

$$C_{kl} - \frac{\delta_{kl}}{\chi(r_k)} = D_{kl}, \tag{8}$$

Eq.(8) results in

$$\sum_{l=1}^{N} D_{kl}\boldsymbol{M}_l = -\boldsymbol{H}_{Sk}, \qquad k = 1,2,...,N. \tag{9}$$

Equation (9) is a governing equation.

2.3. Thin-plate approximation

It is hard to get D_{kl} or C_{kl} in global coordinates because volume integration at each element in the coordinates is hard to be performed. So, after we make *local volume integration* at each element in local coordinates and get D_{kl}', we transform it into D_{kl} in global coordinates by transformation matrix $\left[T_l\right]$ as following,

$$D_{kl} = \left[T_l\right]^{-1} D_{kl}' \left[T_l\right]. \tag{10}$$

The local volume integration was performed for triangular right prism elements that have a certain small thickness as shown in Fig. 2. The flow chart of this analysis is shown in Fig. 3.

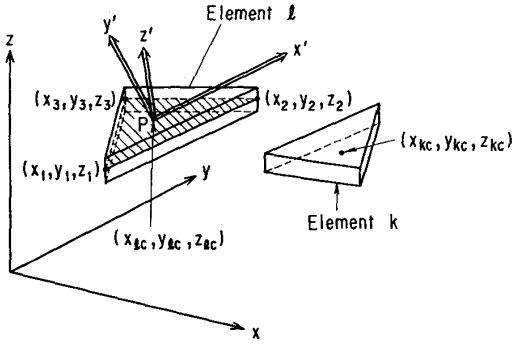

Fig. 2 (a) Local and global coordinates for a triangular right prism element

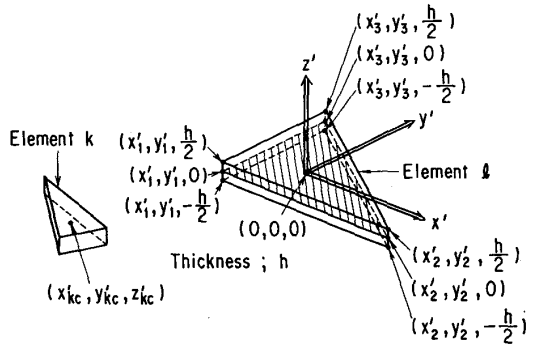

Fig. 2 (b) Local coordinates for a triangular right prism element whose thickness is (h)

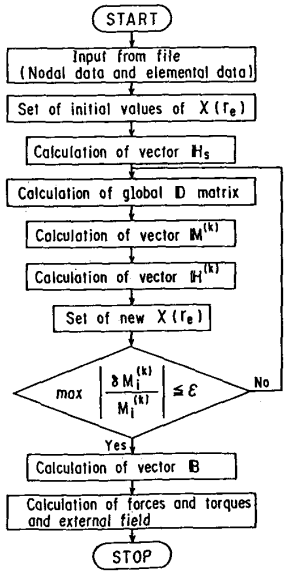

Fig.3 Flow chart of thin-plate approximation analysis (Integral equation method)

3. Verification of This Method

In order to verify the validity of the code based on this method, numerical results were compared with experimental results. Experimental results are quoted from reference 8. When direct current of 25×507 (**AT**) flows in a solenoidal coil, the Z components of magnetic inductions on the R axis and the Z axis are measured both with and without an iron cylinder(circular iron sheet) whose thickness is 1 (**mm**). The experimental model is shown in Fig.4.

In Fig. 5 is shown comparison of magnetic inductions B_z on the R axis between experimental and numerical results. Experimental results with and without the iron cylinder are represented by triangulars and squares, respectively and numerical results by a dash-dotted line and a broken line. Numerical results without the iron cylinder are slightly larger than experimental ones because packing factor of a wire coil is not considered in the numerical analysis. The iron cylinder is divided into 336 triangular elements in the analysis with it. The results were larger than experimental

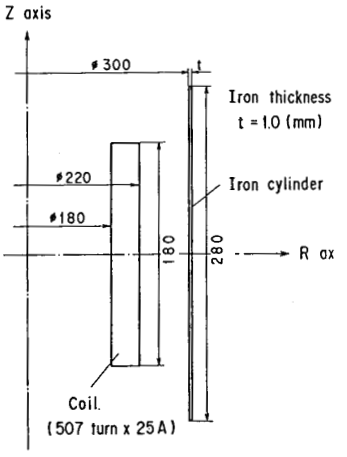

Fig. 4 Experimental model

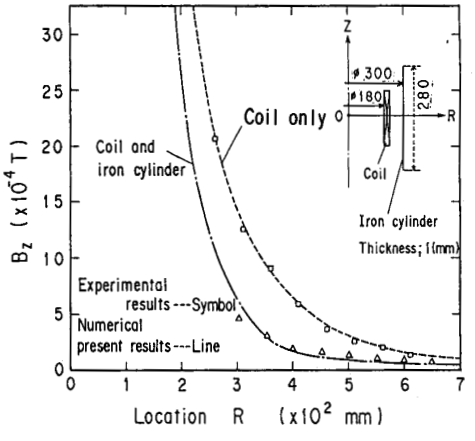

Fig. 5 Comparison of magnetic inductions B_z on the R axis between experimental and numerical results

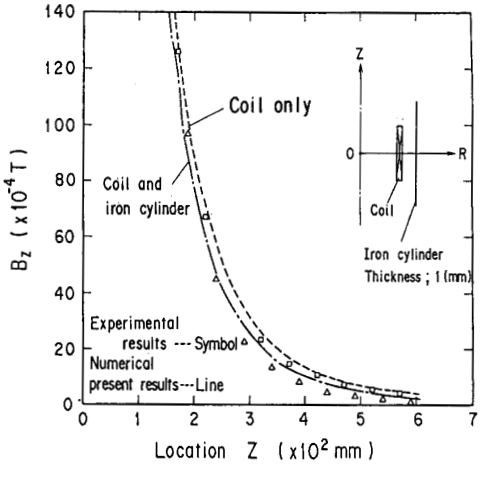

Fig. 6 Comparison of magnetic inductions B_z on the Z axis between experimental and numerical results

ones as the analysis point approached the iron cylinder. This is, we think, because the number of elements is not sufficiently large. The agreement, however, was almost good.

In Fig. 6 is shown comparison of magnetic inductions B_z on the Z axis between experimental and numerical results. The agreement was good in this figure as well as in Fig. 3.

4. Application to SPTR

We applied the method developed here to a ferromagnetic first wall of a fusion power reactor; SPTR which JAERI proposed in 1980 [9] . Its mesh division is shown in Fig. 7. Triangular elements are 80 in the poloidal direction and 4 in the toroidal direction, and the product is 320. The angle per one module in the toroidal direction is 11.25 (deg.) (360(deg.)/32). PF coils current and plasma current in SPTR are shown in Fig.8. Toroidal field $B_T(r)$ is introduced as the following equation,

$$B_T(r) = \frac{35.36}{r} \quad (\mathbf{T}). \tag{11}$$

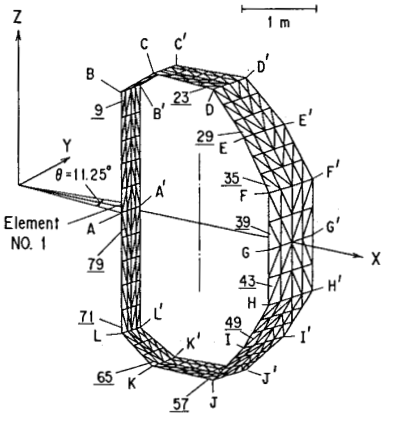

Fig. 7 Mesh division of a ferromagnetic first wall of SPTR

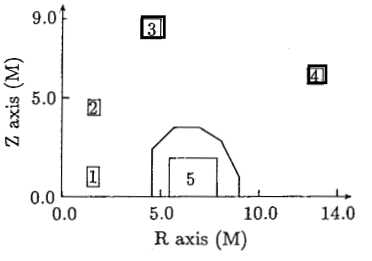

Coil number	Maximum current (MAT)
1	-11.6
2	10.23
3	19.15
4	-12.86
5	16.0

Fig. 8 Locations,cross—sections and current values of poloidal field coils

Distributions of magnetic induction $|B|$ in a first wall both with and without toroidal field are shown in Fig.9. Comparison with the axisymmetric analysis by finite element method was also performed as is shown in Fig. 9. The agreement was good. This figure shows that toroidal field influences magnetic inductions in a ferromagnetic first wall.

We calculated magnetic force $|F|$ in a first wall both with and without toroidal field. As a result we found that magnetic force with toroidal field is about two and a half times larger than one without toroidal field.

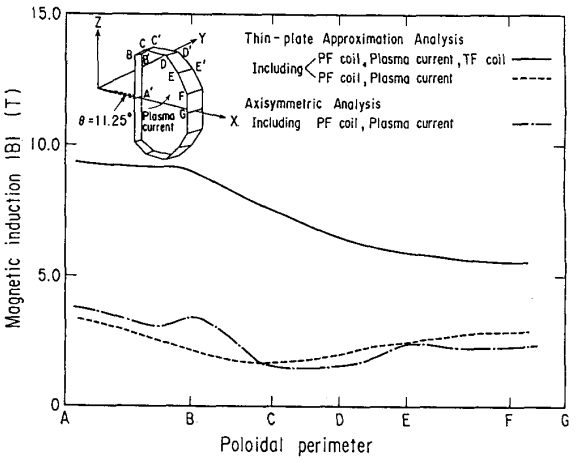

Fig.9 Distribution of magnetic induction |B| in a ferromagnetic first wall of SPTR

Based on these results of magnetic torques and forces we calculated the magnetic stress at the inside surface of a first wall using a structure analysis code SAP-5. The results are shown in Fig. 10.

In addition to poloidal field, this analysis considered toroidal field. Since the field is large at the inboard side, an inboard wall is constrained strongly. From this figure, we can predict that maximum magnetic stress is about 20 **(MPa)** under all the field.

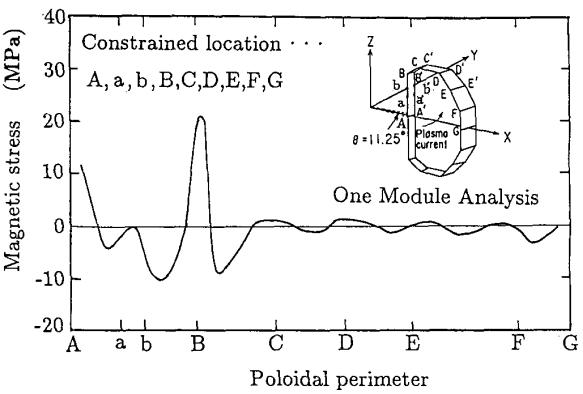

Fig. 10 Distribution of magnetic stress at inside surface of a first wall

5. Conclusion

The following conclusions were obtained in this study.

(1)We have developed a thin plate approximation analysis method to calculate magnetic field in three dimensional complicated components formed by thin shells.

(2)The agreement between numerical results and experimental ones was good, which confirmed the validity of this method.

(3)Application of this method to a ferromagnetic first wall of SPTR was performed. We found that magnetic stress in a wall which is located in the high magnetic field by PF coils, plasma current and TF coils would be less than about 20 **(MPa)** and that the wall could be used in fusion reactor without much problem.

References

[1] K.Miyata and K.Miya, "*Magnetic field and stress analysis of saturated steel*", IEEE, Trans. Mag. 24(1988)pp.230-233

[2] T.Oohira, K.Miyata, T.Takagi, K.Miya, T.Horie, Y.Seki, "*Numerical analysis of purturbed magnetic fields and stress caused by a ferromagnetic first wall*", Fusion Engineering and Design, 1989 Vol.9(1989)pp.95-100

[3] T.Takagi, T.Oohira, K.Miya, "*Magnetic field and stress analysis for a ferromagnetic material*", Applied Electromagnetics in Materials edited by K.Miya, Pergamon Press, Proceedings of the First International Symposium, Tokyo, October 3-5,1988,pp.47-58

[4] P.P.Silvester and R.L.Ferrari, "*Finite Elements for Electrical Engineers*", Cambridge University Press, (1983)pp.111

[5] Ch.Magele, et al., "*Comparison of different finite element formulations for 3D magnetostatic problems*", IEEE, TRANS., MAG-**24**, No.1,(1988)pp.31-34

[6] Ch.Magele and W.Renhart, "*Comparison of the vector potential method with the reduced and total scalar potential method for the analysis of magnetostatic field problems*", IGTE Symposium, (1985)pp.47-54

[7] M.J.Newman,C.W.Trowbridge and L.R.Turner, "*GFUN : An interactive program as an aid to magnet design*", Proceedings of the 4th International Conference on Magnet Technology, Brookhaven, pp.617-626

[8] T.Take and M.Fujita, "*Analysis of cylindrical magnetic field by integral equation method*", IEE. of Jpn. Seishiki Kenkyukai, SA-88-39, RM-88-61, (1988)(Japanese)

[9] T.Tone et. al., "*A Study of the Reactor Structure Concept of the Tokamak Power Reactor SPTR-P*", JAERI Report, M83-031 (March 1983)